Eur. J. Mineral.
2010, **22**, 393–402
Published online April 2010

Saneroite: chemical and structural variations of manganese pyroxenoids with hydrogen bonding in the silicate chain

MARIKO NAGASHIMA* and THOMAS ARMBRUSTER

Mineralogical Crystallography, Institute of Geological Sciences, University of Bern, Freiestrasse 3, CH-3012 Bern, Switzerland
*Corresponding author, e-mail: piemontite7846@gmail.com

Abstract: Saneroite, $Na_{1-1.5}Mn_5[Si_5O_{14}(OH)](Si,V,As)O_3(OH)$ ($Z = 2$, space group $P\bar{1}$), has only been reported from two localities: (1) Val Graveglia, Italy, and (2) Fianel, Switzerland. Samples from both localities were studied using electron-microprobe analysis (EMPA), semi-quantitative analysis of the Mn^{2+}/Mn^{3+} ratio based on the ratio of the X-ray intensities of the Mn L_β and Mn L_α lines, and single-crystal X-ray diffraction methods. The structure has two Na sites (Na1 and Na2), which are 8-coordinated by O. Na1 is fully occupied whereas Na2 is partially occupied. Five crystallographically independent octahedral sites are occupied by Mn (mainly Mn^{2+} with 10–20 % Mn^{3+}), with additional small amounts of Ca and V^{3+}. An undulating pyroxenoid-like chain is built by five SiO_4 tetrahedra. A sixth tetrahedron, forming a branch of the chain, is occupied by V^{5+}, Si^{4+} and As^{5+}. Structure refinements converged to R_1 values of 2.47–2.89 %. In agreement with bond-valence analyses, OH groups are found at the O7 and O19 positions. The relationships between donor and acceptor oxygen atoms and their hydrogen bonds in saneroite are O19–H19···O16 and O7–H7···O11. The O19···O16 and O7···O11 distances are 2.868(2)–2.876(2) and 2.475(2)–2.477(2) Å, respectively. The latter hydrogen bond is extremely short and strong. Corresponding strong hydrogen-bonds were also found in scheuchzerite and several hydrous pyroxenoids with 3- and 5-periodic chains.

Key-words: saneroite, pyroxenoid, Fianel, Molinello, hydrogen bond, crystal structure, scheuchzerite.

1. Introduction

Silicate minerals that have crystallized at low temperature are commonly hydrous and complex both structurally and chemically. Owing to the compositional heterogeneity and the small size of crystals, the crystal structure of these minerals has frequently not been adequately studied. Several Mn-rich hydrous minerals formed by low-grade metamorphism and hydrothermal activity are known to have (V, As)O_4 tetrahedral sites, *i.e.* ardennite, medaite, tiragalloite, fianellite and scheuchzerite. An additional mineral is saneroite, with the simplified formula $Na_{1-1.5}Mn_5[Si_5O_{14}(OH)](Si,V,As)O_3(OH)$ ($Z = 2$). The occurrence of saneroite is scarce and it has been reported from two localities: (1) Val Graveglia, including the Gambatesa and Molinello mines, Genova, Liguria, Italy (type locality; Cortesogno *et al*., 1979; Basso & Della Giusta, 1980; Lucchetti *et al*., 1981), and (2) the Fianel mine, Val Ferrera, Graubünden, Switzerland (Brugger & Berlepsch, 1996; Brugger *et al*., 2006). The crystal structure, space group is *P*, was solved by Basso & Della Giusta (1980) using a specimen from Val Graveglia. There are two independent Na sites, and both are eight-coordinated by O. The Na1 site is fully occupied whereas the Na2 site is only partially occupied. Five crystallographically independent Mn octahedra form a ribbon. These octahedral sites are mainly occupied by Mn^{2+} with small amounts of Mn^{3+}. Five SiO_4 tetrahedra are corner-linked to form a single chain with five tetrahedra in the repeat unit (*fünfereinfach-chain*). One additional tetrahedral site forming a branch of the chain is occupied by V^{5+}, Si^{4+} and As^{5+}.

In this study, we investigated the crystal chemistry of three saneroite crystals from two localities in order to examine structural and compositional variations and to establish the position of one undetermined hydrogen site. The following experimental methods were used: electron-microprobe analysis (EMPA), semi-quantitative analysis of Mn^{2+}/Mn^{3+} ratio using the ratio of the X-ray intensities of the Mn L_β and Mn L_α lines, and single-crystal X-ray diffraction methods. A bond-valence analysis was also carried out. Furthermore, the geometrical features of hydrous and anhydrous pyroxenoids are discussed.

2. Experimental methods

2.1. Samples

(1) Two hand specimens from the manganese mine at Molinello, Val Graveglia, Liguria, Italy (Cortesogno

DOI: 10.1127/0935-1221/2010/0022-2017
0935-1221/10/0022-2017 $ 4.50

et al., 1979; Basso & Della Giusta, 1980; Lucchetti *et al*., 1981) were studied. This locality is in close proximity to the Gambatesa mine. (2) A specimen from the manganese ore deposit in Val Ferrera, Graubünden, Switzerland (Brugger & Berlepsch, 1996) was analyzed. Val Ferrera is the type locality of fianelite, $Mn_2V(V, As)O_7 \cdot 2H_2O$ (Brugger & Berlepsch, 1996) and scheuchzerite, $Na(Mn,Mg)_9[VSi_9O_{28}(OH)](OH)_3$ (Brugger *et al*., 2006). Saneroite occurs as platy crystals up to 2 mm in maximum dimension. The crystals are reddish orange and pleochroic from yellow to dark orange in plane-polarized light.

2.2. Chemical analysis (EMPA)

The chemical composition of saneroite was determined using a JEOL JXA-8200 electron probe microanalyzer at the University of Bern. The abundances of Si, Ti, Al, Cr, V, Fe, Mn, Mg, Ca, Na, K, Cu, Ni and As were measured using an accelerating voltage of 15 kV and a beam current of 2 nA, with a beam diameter of 10 μm. The following standards were used: natural wollastonite (Si, Ca), synthetic ilmenite (Ti), anorthite (Al), synthetic eskolaite (Cr), synthetic shcherbinaite (V), synthetic almandine (Fe), synthetic tephroite (Mn), synthetic spinel (Mg), natural albite (Na), natural orthoclase (K), natural tennantite (Cu), synthetic bunsenite (Ni), and natural arsenopyrite (As). The PRZ method (modified ZAF) with $\phi(\rho Z)$ integration for the atomic number correction (Packwood & Brown, 1981; Bastin *et al*., 1984, 1986) was used for data correction.

Semi-quantitative Mn^{2+}/Mn^{3+} ratios in saneroite were determined using the ratio of the X-ray intensities of the Mn L_β and Mn L_α lines after the method of Albee & Chodos (1970) and Kimura & Akasaka (1999). X-ray intensities were measured with a JXA-8200 electron-probe microanalyzer using a thallium acid phthalate (TAP) monochromator for a range of *L*-values between 206 and 213 mm with a step interval of 0.05 mm and a step counting time of 10 s. The *L*-values are the distances between the measuring spot on the sample and the point on the TAP crystal where the X-ray beam impinges, and are related to the wavelength of X-rays (λ in Å) by the equation

$$L = \frac{R}{d} \times n\lambda$$

where R is the radius of the Rowland circle ($R = 140$ mm), d the (001) interplanar spacing (Å) of the TAP crystal, and n the order of Bragg reflection. The measured spectra were fitted with Lorentzian curves by least-squares methods to determine peak positions, peak widths and peak intensities using a program written by Kimura & Akasaka (1999). The equation,

$$\frac{I(\mathrm{Mn}L_\beta)}{I(\mathrm{Mn}L_\alpha)} = 0.46 \times \frac{\mathrm{Mn}^{2+}}{(\mathrm{Mn}^{2+} + \mathrm{Mn}^{3+})} + 0.554$$

relating peak intensities I to Mn^{2+} and Mn^{3+} contents (Kimura & Akasaka, 1999) was employed.

2.3. Single-crystal X-ray structure analysis

X-ray diffraction data for single-crystals of saneroite were collected using a Bruker SMART APEX II CCD diffractometer of Bruker AXS K.K. Crystals were mounted on glass fibers and intensity data were measured at room temperature using graphite-monochromatized Mo$K\alpha$ radiation ($\lambda = 0.71069$ Å). Preliminary lattice parameters and an orientation matrix were obtained from three sets of frames and refined during the integration process of the intensity data. Diffraction data were collected with ω scans at different φ settings (φ-ωscan) (Bruker, 1999). Data were processed using SAINT (Bruker, 1999). An empirical absorption correction using SADABS (Sheldrick, 1996) was applied. As reported by Basso & Della Giusta (1980), $P\bar{1}$ is the correct space group. Structural refinement was performed using SHELXL-97 (Sheldrick, 1997). Scattering factors for neutral atoms were employed. As^{5+} on T6 was fixed based on the average chemical compositions whereas V and Si on T6 were refined with a restraint of V + Si = 1 – As. Positions of the hydrogen atoms of the hydroxyl groups were derived from difference-Fourier syntheses. Subsequently, hydrogen positions were refined at a fixed value of $U_{iso} = 0.05$ Å^2 and a bond distance restraint of O–H = 0.98(1) Å (Franks, 1973).

3. Results

3.1. Chemical compositions of saneroite

The average chemical compositions of the studied three saneroite samples from two different localities are given in Table 1 where total Mn and V is reported as MnO, V_2O_5, respectively. A result of 2*p* X-ray absorption spectroscopy showed that saneroite from Gambatesa mine (Sample No. BM. 1984, 868) contains both V^{3+} and V^{5+} (Schofield *et al*., 1995). Saneroite displays a zonal growth pattern characterized by Si ↔ V substitution (Fig. 1). The typical zonation observed in all samples shows cores of Si-rich saneroite overgrown by V-rich saneroite. Mn^{2+}/Mn^{3+} analyses (Kimura & Akasaka, 1999) of saneroite samples from Molinello specimens 1 and 2, and Fianel yield 73, 88 and 78–82 % Mn^{2+}, respectively (Fig. 2). Given the low accuracy of this method (±10 %), 10–20 % of total Mn may be trivalent. Calculated bond valences (Basso & Della Giusta, 1980) suggest two hydroxyl groups per formula unit. However, the estimated OH content is often beyond two, if all Mn ions are assumed divalent. This implies the presence of Mn^{3+} in saneroite, which is also supported by own analyses and 2*p* X-ray absorption spectroscopy (Schofield *et al*., 1995). The procedure to construct the chemical formula is as follows: (1) the total number of cations, except Na, K and H ions, is normalized to 11; (2) all Si and As are assigned to the tetrahedral sites including T6; (3) tetrahedral V^{5+} is calculated as 6 – (Si + As), and excess V is assigned to the octahedral sites as V^{3+}; (4) the elements excluding Na (+ K) and tetrahedral cations are assigned to octahedral sites, (5) Na (+ K) is assigned to

Table 1. Average chemical compositions of the saneroite samples (*n*, number of analytical points).

	Molinello, Italy				Fianel, Switzerland	
	Specimen 1		Specimen 2			
Sample No.	1		2		3	
	Ave.	Std.	Ave.	Std.	Ave.	Std.
	$n = 23$		$n = 28$		$n = 30$	
SiO_2	39.99	1.06	39.06	0.65	41.03	0.98
Al_2O_3	0.02	0.00	0.01	0.02	0.01	0.02
MnO	42.20	1.38	40.33	1.06	41.53	1.12
MgO	0.01	0.02	0.00	0.00	0.03	0.04
CaO	0.13	0.05	0.11	0.04	0.33	0.12
Na_2O	4.34	0.28	4.36	0.27	4.52	0.25
K_2O	0.00	0.01	0.01	0.01	0.01	0.01
CuO	0.10	0.14	0.20	0.24	0.14	0.20
NiO	0.03	0.04	0.03	0.03	0.02	0.03
V_2O_5	7.15	1.80	7.78	0.70	6.05	1.23
As_2O_5	1.22	1.27	1.92	1.65	1.31	1.85
Total	95.19		93.81		94.98	
Total cations except for Na + K = 11						
Si	5.41	0.15	5.39	0.11	5.54	0.30
Al	0.00	0.00	0.00	0.00	0.00	0.00
Mn^{2+}	4.83	0.11	4.72	0.10	4.75	0.10
Mg	0.00	0.00	0.00	0.00	0.01	0.01
Ca	0.02	0.01	0.02	0.01	0.05	0.02
Na	1.14	0.08	1.17	0.08	1.18	0.06
K	0.00	0.00	0.00	0.00	0.00	0.00
Cu	0.01	0.01	0.02	0.03	0.02	0.02
Ni	0.00	0.00	0.00	0.00	0.00	0.00
V^{5+}	0.64	0.14	0.71	0.05	0.54	0.09
As^{5+}	0.09	0.09	0.14	0.12	0.09	0.13
Total	12.14		12.17		12.18	

[a]Mn as MnO, V as V_2O_5 and As as As_2O_5.

1: $Na_{1.14}(Mn^{2+}_{4.70}Mn^{3+}_{0.13}Ca_{0.02}Cu_{0.01}V^{3+}_{0.14})_{\Sigma 5.00}[Si_{5.00}O_{14}(OH)](Si_{0.41}V^{5+}_{0.50}As^{5+}_{0.09})O_3(OH)$.

2: $Na_{1.17}(Mn^{2+}_{4.72}Ca_{0.02}Cu_{0.02}V^{3+}_{0.24})_{\Sigma 5.00}[Si_{5.00}O_{14}(OH)](Si_{0.39}V^{5+}_{0.47}As^{5+}_{0.14})O_3(OH)$.

3: $Na_{1.18}(Mn^{2+}_{4.56}Mn^{3+}_{0.19}Ca_{0.05}Cu_{0.02}V^{3+}_{0.17})_{\Sigma 5.00}[Si_{5.00}O_{14}(OH)](Si_{0.54}V^{5+}_{0.37}As^{5+}_{0.09})O_3(OH)$.

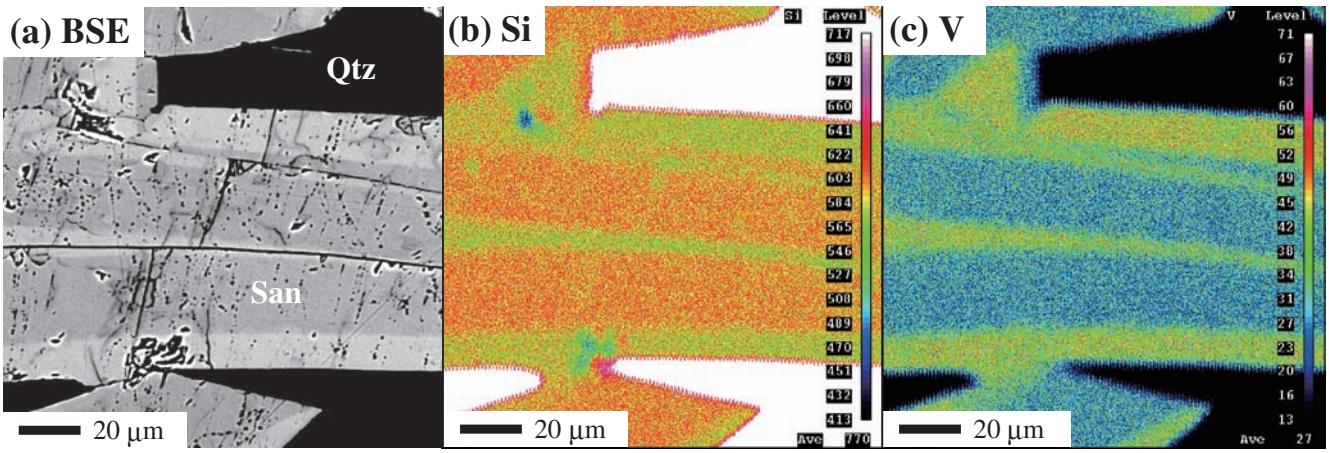

Fig. 1. Backscattered electron (BSE) image (a) and X-ray map images showing the distribution of Si (b) and V (c) in saneroite from Fianel, Switzerland. Abbreviations: San = saneroite, Qtz = quartz. Scale bar is 20 μm.

the eight-coordinated polyhedra, and (6) the Mn^{2+}/Mn^{3+} ratio is calculated to obtain 2OH groups per formula unit (pfu). The corresponding crystal-chemical formulae are: $Na_{1.14}(Mn^{2+}_{4.70}Mn^{3+}_{0.13}Ca_{0.02}Cu_{0.01}V^{3+}_{0.14})_{\Sigma 5.00}$ $[Si_{5.00}O_{14}(OH)](Si_{0.41}V^{5+}_{0.50}As^{5+}_{0.09})O_3(OH)$ (Molinello, specimen1), $Na_{1.17}(Mn^{2+}_{4.72}Ca_{0.02}$ $Cu_{0.02}$ $V^{3+}_{0.24})_{\Sigma 5.00}$ $[Si_{5.00}O_{14}(OH)](Si_{0.39}V^{5+}_{0.47}As^{5+}_{0.14})O_3(OH)$ Molinello, specimen 2), and $Na_{1.18}$ $(Mn^{2+}_{4.56}$ $Mn^{3+}_{0.19}$ $Ca_{0.05}$ $Cu_{0.02}$

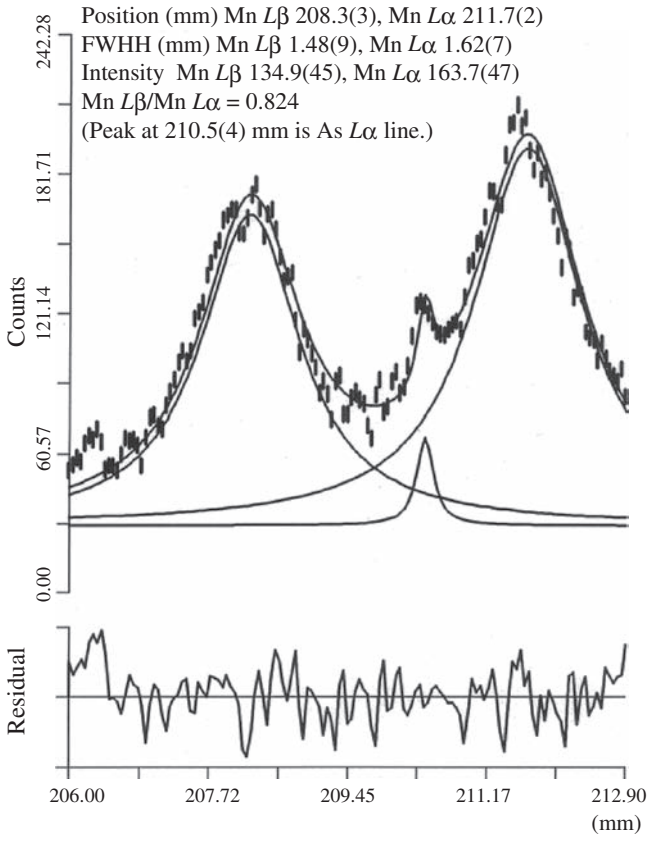

Fig. 2. Microprobe wavelength scans and fitted pattern for L_α and L_β emission peaks of Mn in saneroite from Fianel, Switzerland.

$V^{3+}_{0.17})_{\Sigma 5.00}[Si_{5.00}O_{14}(OH)](Si_{0.54}V^{5+}_{0.37}As^{5+}_{0.09})O_3(OH)$ (Fianel, Switzerland).

3.2. Crystal-structure solution and refinements

Crystallographic data and refinement parameters are summarized in Table 2. The refined atomic positions and anisotropic mean square displacement parameters are listed in Tables 3[1] and 4[1] (deposited and freely available on the GSW site of the journal at http://eurjmin.geoscienceworld.org). The site occupancies of cation sites are summarized in Table 5. Interatomic distances and angles are presented in Tables 6 and 7[1], (deposited and freely available on the GSW site of the journal at http://eurjmin.geoscienceworld.org) respectively. The crystal structure of saneroite is shown in Fig. 3a.

Unit-cell parameters of saneroite from both localities vary in a very narrow range (Table 1) and they are close to those reported by Basso & Della Giusta (1980) and Lucchetti *et al*. (1981). Structure refinements in this study converged to R_1 values of 2.47–2.89 %.

According to the measured site-scattering values, Na fully occupies Na1 whereas the Na2 site is only partially occupied by Na (54–63 %). These results are consistent with a previous study (Basso & Della Giusta, 1980).

According to the chemical analyses, several elements, such as V, Ca, Cu, Ni, Mg, must be assigned to octahedral sites. However, it was impossible to determine their distribution among the octahedra. Although site occupancies of all octahedral sites were initially refined without any restraints, they showed full occupancy by Mn within standard deviation. Thus, Mn1 to Mn5, were fixed at 1.0 Mn during final refinements. Based on octahedral volumes (Table 6), it may be suggested that cations smaller than Mn^{2+} (0.83 Å), such as V^{3+} (0.64 Å) and Mn^{3+} (0.645 Å), occupy the Mn2, Mn3 and Mn4 sites, whereas Ca (1.00 Å) ions may favor Mn1 and Mn5.

Tetrahedral sites T1–T5 are fully occupied by Si. On the other hand, T6 is occupied by a mixture of Si, V and As. Based on the result of the chemical analysis, the Si content of T6 can be estimated as 20–80 %. As result of structural refinements, the dominant cation in T6 in all crystals is V.

Bond-valence sums were calculated using the electrostatic strength function of Brown & Altermatt (1985) and the bond-valence parameters of Brese & O'Keeffe (1991). The results are given in Table 8. The calculated bond-valence sums and refined hydrogen positions indicate that one hydroxyl group is located at O19 (Basso & Della Giusta, 1980) with O16 acting as acceptor. The bond-valence sums of O7 and O11 are both 1.6 valence units (Table 8). As a result of our structural refinements, O7–H7 forms the second hydroxyl group and O11 acts as acceptor. O7···O11 has already been predicted as hydrogen bond based on the bond-valence sums (Basso & Della Giusta, 1980), the hydrogen position, however, could not be resolved in their study.

4. Discussion

4.1. Normalization of chemical composition

A simplified formula of saneroite can be represented as $Na_{1-1.5}Mn_5[Si_5O_{14}(OH)](Si, V, As)O_3(OH)$ ($Z = 2$). Based on chemical analyses, the maximum As content in this study was 0.46 pfu. Lucchetti *et al*. (1981) suggested Si + V + As = 6 as normalization for the chemical formula (in their paper Si + V + As = 12, $Z = 1$). However, the result of 2*p* X-ray absorption spectroscopy showed that vanadium ions in saneroite exist as tetrahedral V^{5+} and octahedral V^{3+} (Schofield *et al*., 1995). Thus, a normalization based on tetrahedral cations, $\Sigma(Si + V + As) = 6$, should not be used. Instead a total of 11 cations pfu (including tetrahedra and octahedra but excluding K, Na and H ions) is obviously a more appropriate normalization scheme.

For all three structurally investigated crystals, the dominant cation in T6 is V^{5+}. On the other hand, the average chemical formula of saneroite from Fianel, Switzerland shows Si-dominance on T6 (Table 1). Although the Si/V ratio of the T6 site in saneroite was defined as 1:1 (Basso & Della Giusta, 1980), chemical analyses indicate variable Si/V ratios and an additional As content. This implies that Si and As may also be the dominant cations in T6. The chemical formulae of Si and As dominant analytical points are:$Na_{1.14}(Mn^{2+}_{4.26}Mn^{3+}_{0.54}$

Table 2. Data collection and details of structure refinement.

	Molinello, Italy		
	Specimen 1	Specimen 2	Fianel, Switzerland
Space group	$P\bar{1}$	$P\bar{1}$	$P\bar{1}$
Crystal size (mm)	0.16 × 0.08 × 0.05	0.10 × 0.03 × 0.01	0.135 × 0.05 × 0.025
Cell parameters			
a (Å)	9.7467(1)	9.7515(1)	9.7510(1)
b (Å)	9.9649(2)	9.9678(2)	9.9687(2)
c (Å)	9.1065(1)	9.1173(1)	9.1185(1)
α (°)	92.653(1)	92.601(1)	92.580(1)
β (°)	117.179(1)	117.230(1)	117.214(1)
γ (°)	105.304(1)	105.304(1)	105.334(1)
V (Å^3)	744.42(6)	745.66(6)	745.82(6)
Dcalc (g/cm^3)	3.45	3.46	3.44
Absorption coefficient μ (mm^{-1})	7.20	7.19	7.19
Corrected reflections	30,490	31,040	32,943
Unique reflections	6572	4539	6500
Criterion for observed reflections	$I > 2\sigma(I)$	$I > 2\sigma(I)$	$I > 2\sigma(I)$
R_{int} (%)	2.66	4.76	2.97
R_σ (%)	2.22	3.62	2.61
θ_{max} (°)	35.1	30.5	35.2
Miller index limit	$-15 \le h \le 15, -16 \le k \le 16, -14 \le l \le 14$	$-13 \le h \le 13, -14 \le k \le 14, -13 \le l \le 13$	$-15 \le h \le 15, -15 \le k \le 16, -14 \le l \le 14$
R_1 (%)	2.47	2.89	2.65
$wR2$ (%)	6.06	6.93	6.38
S	1.196	1.057	1.081
No. of parameters	296	296	295
Weighting scheme	$w = 1/[\sigma^2(F_o^2) + (0.0153P)^2 + 0.90P]$	$w = 1/[\sigma^2(F_o^2) + (0.0258P)^2 + 0.66P]$	$w = 1/[\sigma^2(F_o^2) + (0.0224P)^2 + 0.79P]$
$\Delta\rho_{max}$ (e Å^{-3})	0.590 (0.79Å from O17)	0.608 (0.52Å from O5)	0.95 (1.76Å from O6)
$\Delta\rho_{min}$ (e Å^{-3})	–0.444 (1.12 Å from T6)	–0.632 (1.17 Å from T3)	–0.55 (0.70 Å from T1)

Notes: X-ray diffraction data were collected using a Bruker SMART APEX II CCD diffractometer. Intensity data were measured at room temperature using graphite-monochromatized Mo$K\alpha$ radiation ($\lambda = 0.71069$ Å). Diffraction data were collected with φ-ω scans (Bruker, 1999). Data were processed using SAINT (Bruker, 1999). An empirical absorption correction using SADABS (Sheldrick, 1996) was applied. Structural refinement was performed using SHELXL-97 (Sheldrick, 1997). The function of the weighting scheme is $w = 1/(\sigma^2(F_o^2) + (a \cdot P)^2 + b \cdot P)$, where $P = (\mathrm{Max}(F_o^2, 0) + 2F_c^2)/3$, and the parameters a and b are chosen to minimize the differences in the variances for reflections in different ranges of intensity and diffraction angle.

Table 5. Site occupancies of the saneroite samples[a].

	Molinello, Italy		
Site	Specimen 1	Specimen 2	Fianel, Switzerland
Na1	Na1.0	Na1.0	Na1.0
Na2	Na0.568(4)	Na0.537(5)	Na0.625(4)
T1	Si1.0	Si1.0	Si1.0
T2	Si1.0	Si1.0	Si1.0
T3	Si1.0	Si1.0	Si1.0
T4	Si1.0	Si1.0	Si1.0
T5	Si1.0	Si1.0	Si1.0
T6	Si0.42(2)V0.49(1)As0.09	Si0.34(2)V0.54(1)As0.14	Si0.40(2)V0.52(1)As0.09
Mn1	Mn1.0	Mn1.0	Mn1.0
Mn2	Mn1.0	Mn1.0	Mn1.0
Mn3	Mn1.0	Mn1.0	Mn1.0
Mn4	Mn1.0	Mn1.0	Mn1.0
Mn5	Mn1.0	Mn1.0	Mn1.0

[a]At the primary stage, populations of Na at Na1, Si at T1, T2, T3, T4 and T5, and Mn at Mn1, Mn2, Mn3, Mn4 and Mn5 for all samples were refined. However, these sites turned out to be fully occupied. Thus, the site occupancies at these sites were fixed at 1.0. As^{5+} on T6 was fixed based on the average chemical composition.

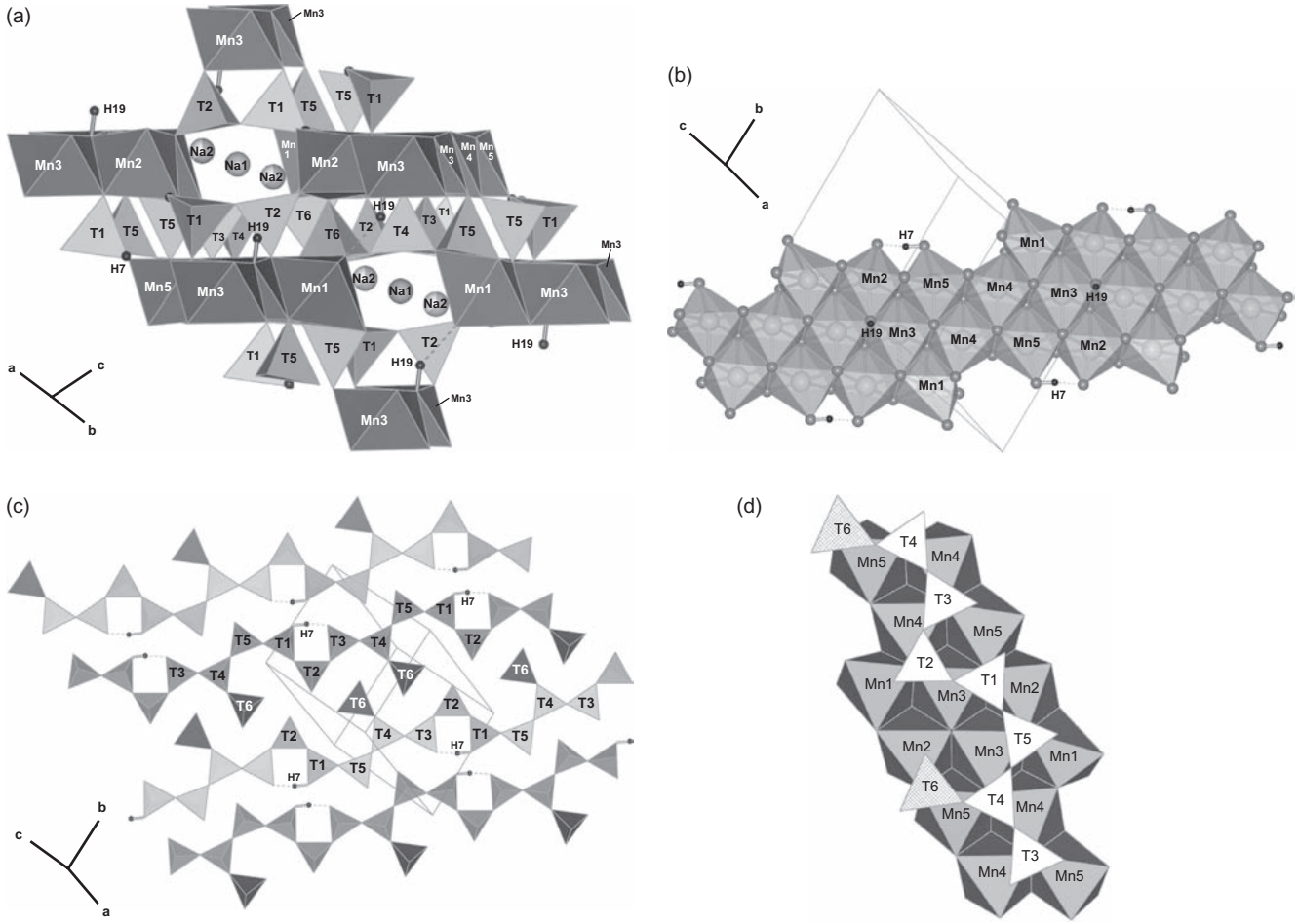

Fig. 3. The crystal structure of saneroite (a), and octahedral layers (b), tetrahedral chains (c), and octahedral bands with silicate chains (d) in the structure of saneroite drawn using the program VESTA (Momma & Izumi, 2008). Dashed lines indicate H···O bonds.

$V^{3+}_{0.13}Ca_{0.02}Cu_{0.01}Ni_{0.01}\ Al_{0.01}\ Mg_{0.01})_{\Sigma 5.00}\ [Si_{5.00}\ O_{14}(OH)]\ (Si_{0.79}V^{5+}_{0.21})O_3(OH)$ and $Na_{1.12}(Mn^{2+}_{4.61}V^{3+}_{0.32}Ca_{0.05}Mg_{0.01}Cu_{0.01}\ \ Ni_{0.01})_{\Sigma 5.00}Si_{5.00}O_{14}(OH)](Si_{0.46}V^{5+}_{0.08}As^{5+}_{0.46})O_3$ (OH), respectively. In the future, if more saneroite occurrences have been found, it might be advisable to define new species with the dominant cation in T6 added as suffix, *i.e.* ''saneroite-(V)'', ''saneroite-(Si)'' and ''saneroite-(As)'', as recently approved for ardennite with $V^{5+} > As^{5+}$, which has been named ardennite-(V) (Barresi *et al*., 2007).

4.2. Structural variation and hydrogen bonds

Compositional and structural similarities between saneroite and scheuchzerite ($Z = 1$, space group $P\bar{1}$, $Na(Mn,Mg)_9[VSi_9O_{28}(OH)](OH)_3$) were pointed out by Brugger *et al*. (2006). [$Mn(O,OH)_6$] octahedra in the structures of both minerals form ribbons, which have different topologies (2-2-3-3 in saneroite; 3-3-4-4-4 in scheuchzerite; Fig. 3b in this study and Fig. 5 in Brugger *et al*., 2006). The saneroite silicate single-chain has five tetrahedra in the repeating unit and it features an additional tetrahedron branching sideways (Fig. 3c). In contrast, the scheuchzerite chain consists of the branched saneroite chain with four additional attached silicate tetrahedra. Saneroite is categorized as a member of the *p-p* (pectolite-pyroxene) series defined by Takéuchi & Koto (1977). The pyroxenoids of the *p-p* series are chemically characterized by hydrogen atoms and additional monovalent cations (Takéuchi & Koto, 1977), *i.e.* Na in saneroite. In saneroite, the upper triangular face of the center tetrahedron (T2) in the C-shaped tetrahedral triplet and the upper triangular faces of octahedra (Mn1, Mn3 and Mn4) share the basal oxygen (O10) of the center tetrahedron. The upper triangular faces of the tetrahedron and octahedra are pointing in opposite directions (Fig. 3d). This topological feature also meets the characteristic requirements of the *p-p* series (Takéuchi & Koto, 1977; Mellini & Merlino, 1982). The topology of the scheuchzerite structure is reminiscent of *p-p* series pyroxenoids. However, the chain contains also ''loops'' as defined by Brugger *et al.* (2006). In this sense the structure of scheuchzerite is exceptional.

The position of hydrogen atoms and directions of the hydrogen bonds in saneroite are shown in Fig. 3. The relationships between donor and acceptor oxygen atoms and their hydrogen bonds are O19–H19···O16 and O7–H7···O11. The O19···O16 and O7···O11 distances

Table 8. Calculated bond valences in the saneroite samples.

Site	Molinello, Italy		Fianel, Switzerland
	Specimen 1	Specimen 2	
Na1	0.98	0.96	0.96
Na2	0.81	0.75	0.89
Mn1	1.90	1.91	1.89
Mn2	2.02	2.01	1.98
Mn3	2.03	2.01	2.02
Mn4	1.96	1.96	1.96
Mn5	1.92	1.91	1.90
T1	4.18	4.20	4.18
T2	4.07	4.15	4.14
T3	4.20	4.21	4.20
T4	4.21	4.23	4.21
T5	4.14	4.14	4.15
T6	4.57	5.07	4.76
O1	2.18	2.18	2.18
O2	2.07	2.07	2.06
O3	2.11	2.13	2.13
O4	2.26	2.24	2.28
O5	2.19	2.19	2.18
O6	2.15	2.25	2.19
O7	1.60	1.60	1.60
O8	1.92	1.94	1.93
O9	1.98	1.98	1.97
O10	1.92	1.98	1.98
O11	1.60	1.60	1.60
O12	2.00	2.01	2.00
O13	2.05	2.03	2.04
O14	1.91	1.91	1.92
O15	2.00	2.00	2.00
O16	1.74	1.88	1.79
O17	1.91	2.00	1.92
O18	1.79	1.92	1.88
O19	1.12	1.12	1.11

are 2.868(2)–2.876(2) and 2.475(2)–2.477(2) Å, respectively. The latter hydrogen bond is extremely strong. The calculated wavenumber of IR bands is 3478–3485 cm^{-1} for O19···O16 and 1373–1407 cm^{-1} for O7···O11 (Libowitzky, 1999). Brugger *et al*. (2006) compared the ATR-FTIR spectrum of saneroite from Fianel, Switzerland with that of scheuchzerite (see Fig. 2 in their paper). As predicted above, the IR spectrum of saneroite has two O–H stretching modes at *ca.* 3500 cm^{-1} and *ca.* 1400 cm^{-1}. No absorption band was observed around 1600–1650 cm^{-1}, which would correspond, if present, to the bending mode of H_2O. Thus, there is no molecular water in saneroite. Scheuchzerite and saneroite are also topologically very similar. In both structures, the hydrogen-bond is very strong, and it exists at the open side of the C-shaped tetrahedral triplet (Ohashi & Finger, 1981). The hydrogen bond is bridging T1 and T3 tetrahedra in saneroite (Fig. 3c), and Si2 and Si4 in scheuchzerite (see Figure 4(a) in Brugger *et al*., 2006). In case of saneroite, the hydroxyl group O7–H7 is at the common corner of the $T1O_4$ tetrahedron and the $Mn5O_6$ octahedron. The hydrogen-bond acceptor is O11. In contrast, positional hydrogen disorder with O26 and O29, occupied by O and OH, in equal proportions was suggested in case of scheuchzerite (Brugger *et al*., 2006). In fact, the O26···O29 distance in scheuchzerite (2.35 Å) is even shorter than O7···O11 in saneroite, which may be the reason for the observed H site disorder. A similar situation of disordered hydrogen was also observed in the pyroxenoid structure of serandite ($NaMn_2[Si_3O_8(OH)]$) having a O···O distance of 2.464–2.468 Å (Jacobsen *et al*., 2000). Correspondingly, the IR O–H stretching mode for serandite was found at 1386 cm^{-1} (Hammer *et al*., 1998).

A comparison of O···O distances at the open side of the C-shaped tetrahedral triplet in hydrous pyroxenoids and anhydrous pyroxenoids is listed in Table 9. The short O···O separation is responsible for extremely strong hydrogen-bonds in hydrous pyroxenoids. The topologically corresponding O···O separation in anhydrous pyroxenoids is longer (3.24–3.62 Å) than that in hydrous pyroxenoids (2.45–2.60 Å). Liebau (1980) showed that hydrogen bonds within the tetrahedral chains lead to marked chain shrinkage due to kinking of the chains in the hydrous pyroxenoids. Similarly, krauskopfite, $BaSi_2O_4(OH)_2{\cdot}2H_2O$ ($Z = 4$, space group $P2_1/a$) described by Coda *et al*. (1967), characterized by a four-periodic single chain, has also two silanol groups. One of them is topologically similar to the hydrogen-bond at the open side of the C-shaped tetrahedral triplet, although the chain in krauskopfite is slightly twisted (Coda *et al*., 1967). This hydrogen bonded O···O distance is *ca.* 2.60 Å, which is slightly longer than those in hydrous pyroxenoids.

The hydrogen bonds of megacyclite, $Na_8K(Si_9O_{18}(OH)_9){\cdot}19H_2O$ ($Z = 4$, space group $P2_1/n$) described by Yamnova *et al*. (1992), are also topologically similar to the short one in krauskopfite. Megacyclite has unusual, large, ring-like groups consisting of 18 SiO_4 tetrahedra, and two of the nine hydroxyl groups have the O–H···O bonds at the open side of the twisted C-shape tetrahedral triplet. These silanol groups belong to the category of tetrahedra with two bridging O atoms to adjacent tetrahedra (Nyfeler & Armbruster, 1998). However, the O–H···O separations, 2.72 and 2.84 Å, are significantly longer than those in pyroxenoids and krauskopfite because of the considerably twisted tetrahedral triplets. Thus, the torsion of the tetrahedral triplet is also an important parameter for the formation of very strong hydrogen-bonds at the open side of the C-shaped tetrahedral moiety.

Nyfeler & Armbruster (1998) used bond-strength arguments to explain why orthosilicates (with no bridging O) have significantly longer Si–OH bonds than the non-hydrogenated remaining <Si–O> distances in the same tetrahedron. In addition, they also showed that tetrahedra with three bridging O have longer Si–OH bonds than the corresponding non-hydrogenated <Si–O> distances. This trend of increased Si–OH distances misled Jacobsen *et al*. (2000) to assume that chain silicates (two bridging O) also have generally lengthened Si–OH bonds. However, pyroxenoids with very short O–H···O distances at the open side of the C-shaped tetrahedral triplet obviously contradict this assumption (*e.g*., Jacobsen *et al*., 2000). Tables 9 and 10 indicate that for hydrous pyroxenoids Si–OH bonds and <Si–O> bond lengths are very similar. The reason is that for very short O–H···O distances (*e.g*., hydrous pyroxenoids) the acceptor oxygen of the hydrogen bond receives

Table 9. Comparison of O···O distances at the open side of the C-shaped tetrahedral triplet in hydrous and anhydrous pyroxenoids.

Hydrous pyroxenoid				Anhydrous pyroxenoid			
Periodicity	Mineral name	O···O distance	Reference[b]	Periodicity	Mineral name	O···O distance	Reference[b]
3	Cascandite	2.597	1	3	Bustamite	3.263	18
3	Pectolite	2.473	2	3	Bustamite	3.237–3.532	2
3	Pectolite	2.482	3	3	Ferrobustamite	3.538	19
3	Serandite	2.454	4	3	Wollastonite-1A	3.588–3.603	2
3	Serandite	2.456	5	3	Wollastonite-1A	3.617	20
3	Serandite	2.470	2	3	Wollastonite-2M	3.617	20
3	Serandite	2.464 – 2.468	6	3	Wollastonite-2M	3.624	21
				3	Wollastonite-2M	3.622	22
5	Babingtonite	2.581	7	3	Sorensenite	3.295	23
5	Babingtonite	2.569	8	3	Sorensenite	3.235	24
5	Babingtonite	2.574	9				
5	Babingtonite	2.563–2.566	10	5	Rhodonite	3.420	25
5	Scandiobabingtonite	2.576	11	5	Rhodonite	3.257	26
5	Nambulite	2.446	12	5	Rhodonite	3.267	27
5	Marsturite	*ca.* 2.5	13	5	Zn-rich rhodonite	3.369	27
5	Li-hydrorhodonite	2.465	14				
5	Santaclaraite	2.491	15	7	Pyroxferroite	3.309	28
5	Saneroite	2.474	16	7	Pyroxmangite	3.368	25
5	Saneroite	2.475 – 2.477	This study	7	Pyroxmangite	3.357	29
				7	Pyroxmangite	3.297	30
	Scheuchzerite[a]	2.379	17				

[a]The topology of the scheuchzerite structure is reminiscent of that of pyroxenoids, but the chain contains loops. Thus, the scheuchzerite structure is unique.
[b]References are as follows: (1) Mellini & Merlino, 1982; (2) Ohashi & Finger, 1978; (3) Prewitt, 1967; (4) Takéuchi *et al*., 1973; (5) Takéuchi *et al*., 1976; (6) Jacobsen *et al*., 2000; (7) Araki & Zoltai, 1972; (8) Kosoi, 1976; (9) Tagai *et al*., 1990; (10) Armbruster, 2000; (11) Orlandi *et al*., 1998; (12) Narita *et al*., 1975; (13) Kolitsch, 2008; (14) Murakami *et al*., 1977; (15) Ohashi & Finger, 1981; (16) Basso & Della Giusta, 1980; (17) Brugger *et al*., 2006; (18) Peacor & Buerger, 1962; (19) Yamanaka *et al*., 1977; (20) Ohashi, 1984; (21) Trojer, 1968; (22) Hesse, 1984; (23) Maksimova *et al*., 1974; (24) Metcalf-Johansen & Grønbæk Hazell, 1976; (25) Narita *et al*., 1977; (26) Peacor *et al*., 1978; (27) Nelson & Griffen, 2005; (28) Burnham, 1971; (29) Pinckney & Burnham, 1988; (30) Zanazzi *et al*., 2008.

Table 10. Si–OH and <Si–O> distances of the tetrahedra in hydrous pyroxenoids having the hydrogen-bond at the open side of the C-shaped tetrahedral triplet.

Periodicity	Mineral name	Si–OH	<Si–O>	Reference[a]
3	Cascandite	1.628(4)	1.623	1
3	Pectolite	1.627(4)	1.626	3
3	Serandite	1.628(1)	1.621	6
5	Babingtonite	1.623(3)	1.628	9
5	Babingtonite	1.616(2)–1.620(2)	1.618–1.620	10
5	Santaclaraite	1.624(2)	1.616	15
5	Saneroite	1.624(1)–1.630(1)	1.622–1.623	This study

[a]Reference numbers are the same as those in Table 9.

a significant bond-valence contribution from the hydrogen bond whereas the bond-valence fraction of the donor oxygen is significantly reduced (Ferraris & Ivaldi, 1988). Thus, the reduced overbonding of the donor oxygen does not necessitate a counterbalancing effect by lengthening Si–OH. In contrast, in krauskopfite (Coda *et al*., 1967) and megacyclite (Yamnova *et al*., 1992) with longer O–H···O distances, the counterbalancing effect is active and Si–OH bond lengths are longer than <Si–O> bonds within the silanol tetrahedra.

Acknowledgements: We thank Prof. E. Tillmanns, chief editor, an anonymous referee for their constructive comments, Prof. M. Akasaka, Shimane University, Japan for his help on this manuscript, and E. Wadoski, University of Bern, for improving the English. This research was supported by the Japan Society for the Promotion of Science (JSPS) for research abroad to M. Nagashima.

References

Albee, A. & Chodos, A.A. (1970): Semiquantitative electron microprobe determination of Fe^{2+}/Fe^{3+} and Mn^{2+}/Mn^{3+} in

oxides and silicates and its application to petrologic problems. *Am. Mineral*., **55**, 491–501.

Araki, T. & Zoltai, T. (1972): Crystal structure of babingtonite. *Z. Kristallogr*., **135**, 355–373.

Armbruster, T. (2000): Cation distribution in Mg, Mn-bearing babingtonite from Arvigo, Val Valanca, Grisons, Switzerland. *Schweiz. Mineral.Petrogr. Mitt*., **80**, 279–284.

Barresi, A.A., Orlandi, P., Pasero, M. (2007): History of ardennite and the new mineral ardennite-(V). *Eur. J. Mineral*., **19**, 581–587.

Basso, R. & Della Giusta, A. (1980): The crystal structure of a new manganese silicate. *N. Jb. Mineral. Abh.*, **138**, 333–342.

Bastin, G.F., van Loo, F.J.J., Heijlingers, H.J.M. (1984): Evaluation of the use of Gaussian $\phi(\rho z)$ curves in quantitative electron probe microanalysis: a new optimization. *X-ray Spectrom.*, **13**, 91–97.

Bastin, G.F., Heijlingers, H.J.M., van Loo, F.J.J. (1986): A further improvement in the Gaussian $\phi(\rho z)$ approach for matrix correction in quantitative electron probe microanalysis. *Scanning*, **8**, 45–67.

Brese, N.E. & O'Keeffe, M. (1991): Bond-valence parameters for solids. *Acta Crystallogr*., **B47**, 192–197.

Brown, I.D. & Altermatt, D. (1985): Bond-valence parameters obtained from a systematic analysis of the inorganic crystal structure database. *Acta Crystallogr*., **B41**, 244–247.

Brugger, J. & Berlepsch, P. (1996): Description and crystal structure of fianelite, $Mn_2V(V, As)O_7{\cdot}2H_2O$, a new mineral from Fianel, Val Ferrera, Graubünden, Switzerland. *Am. Mineral*., **81**, 1270–1276.

Brugger, J., Krivovichev, S., Meisser, N., Ansermet, S., Armbruster, T. (2006): Scheuchzerite, $Na(Mn,Mg)_9[VSi_9O_{28}(OH)](OH)_3$, a new single-chain silicate. *Am. Mineral*., **91**, 937–943.

Bruker (1999): SMART and SAINT-Plus. Versions 6.01. Bruker AXS Inc., Madison, Wisconsin, USA.

Burnham, C.W. (1971): The crystal structure of pyroxferroite from Mare Tranquillitatis. *Proc. Second Lunar Sci. Conf.*, **1**, 47–57.

Coda, A., dal Negro, A., Rossi, G. (1967): The crystal structure of krauskopfite. *Atti Accad. Naz. Lincei, Classe Sci. ische, Matematische Nat., Rend.*, **42**, 859–873.

Cortesogno, L., Lucchetti, G., Penco, A.M. (1979): Le mineralizzazioni a manganese nei diaspri delle ofioliti liguri: mineralogia e genesi. *Rend. Soc. Ital. Mineral. Petrol.*, **35**, 151–197 (in Italian).

Ferraris, G. & Ivaldi, G. (1988): Bond valence *vs* bond length in O···O hydrogen bonds. *Acta Crystallogr*., **B44**, 341–344.

Franks, F., ed. (1973): Water: a comprehensive treatise, Vol. 2. Plenum, New York, 684 p.

Hammer, V.M.F., Libowitzky, E., Rossman, G.R. (1998): Single-crystal IR spectroscopy of very strong hydrogen bonds in pectolite, $NaCa_2[Si_3O_8(OH)]$, and serandite, $NaMn_2[Si_3O_8(OH)]$. *Am. Mineral*., **83**, 569–576.

Hesse, K.F. (1984): Refinement of the crystal structure of wollastonite-2M (parawollastonite). *Z. Kristallogr*., **168**, 93–98.

Jacobsen, S.D., Smyth, J.R., Swope, R.J., Sheldon, R.I. (2000): Two proton positions in the very strong hydrogen bond of serandite, $NaMn_2[Si_3O_8(OH)]$. *Am. Mineral*., **85**, 745–752.

Kimura, Y. & Akasaka, M. (1999): Estimation of Fe^{2+}/Fe^{3+} and Mn^{2+}/Mn^{3+} ratios by electron probe micro analyzer. *J. Mineral. Soc. Japan*, **28**, 159–166 (in Japanese with English abstract).

Kolitsch, U. (2008): Implications for the nomenclature of p-p hydropyroxenoid: the crystal structure of marsturite from the Molinello mine, Italy. *Tagung Dtsch. Mineral. Ges*. (Abstract).

Kosoi, A. (1976): The structure of babingtonite. *Sov. Phys. Crystallogr.*, **20**, 446–451.

Libowitzky, E. (1999): Correlation of O–H stretching frequencies and O–H···O hydrogen bond lengths in minerals. *Mh. Chem.*, **130**, 1047–1059.

Liebau, F. (1980): The role of cationic hydrogen in pyroxenoid crystal chemistry. *Am. Mineral*., **65**, 981–985.

Lucchetti, G., Penco, A.M., Rinaldi, R. (1981): Saneroite, a new natural hydrated Mn-silicate. *N. Jb. Mineral. Mh.*, **1981**, 161–168.

Maksimova, N.V., Ilyukhin, V.V., Belov, N.V. (1974): Crystal structure of sorensenite. *Sov. Phys. Dokl*., **18**, 681–682.

Mellini, M. & Merlino, S. (1982): The crystal structure of cascandite, $CaScSi_3O_8(OH)$. *Am. Mineral*., **67**, 604–609.

Metcalf-Johansen, J. & Grønbæk Hazell, R. (1976): The crystal structure of sorensenite, $Na_4SnBe_2(Si_3O_9)_2.2H_2O$. *Acta Crystallogr*., **B32**, 2553–2556.

Momma, K. & Izumi, F. (2008): VESTA: a three-dimensional visualization system for electronic and structural analysis. *J. Appl. Crystallogr*., **41**, 653–658.

Murakami, T., Takéuchi, Y., Tagai, T. (1977): Lithium-hydrorhodonite. *Acta Crystallogr*., **B33**, 919–921.

Narita, H., Koto, K., Morimoto, N., Yoshii, M. (1975): The crystal structure of nambulite $(Li,Na)Mn_4Si_5O_{14}(OH)$. *Acta Crystallogr*., **B31**, 2422–2426.

Narita, H., Koto, K., Morimoto, N. (1977): The crystal structures of $MnSiO_3$ polymorphs (rhodonite pyroxmangite-type). *Mineral. J*., **8**, 329–342.

Nelson, W.R. & Griffen, D.T. (2005): Crystal chemistry of Zn-rich rhodonite (''fowlerite''). *Am. Mineral*., **90**, 969–983.

Nyfeler, D. & Armbruster, T. (1998): Silanol groups in minerals and inorganic compounds. *Am. Mineral*., **83**, 119–125.

Ohashi, Y. (1984): Polysynthetically-twinned structures of enstatite and wollastonite. *Phys. Chem. Minerals*, **10**, 217–229.

Ohashi, Y. & Finger, L.W. (1978): The role of octahedral cations in pyroxenoid crystal chemistry. I. Bustamite, wollastonite, and the pectolite-schizolote-serandite series. *Am. Mineral*., **63**, 274–288.

—, — (1981): The crystal structure of santaclaraite, $CaMn_4[Si_5O_{14}(OH)](OH){\cdot}H_2O$: the role of hydrogen atoms in the pyroxenoid structure. *Am. Mineral*., **66**, 154–168.

Orlandi, P., Pasero, M., Vezzalini, G. (1998): Scandiobabingtonite, a new mineral from the Baveno pegmatite, Piedmont, Italy. *Am. Mineral*., **82**, 1330–1334.

Packwood, R.H. & Brown, J.D. (1981): A Gaussian expression to describe $\phi(\rho z)$ curves for quantitative electron probe microanalysis. *X-ray Spectrom.*, **10**, 138–146.

Peacor, D.R. & Buerger, M.J. (1962): Determination and refinement of the crystal structure of bustamite, $CaMnSi_2O_6$. *Z. Kristallogr*., **117**, 313–343.

Peacor, D.R., Essene, E.J., Brown, P.E., Winter, G.A. (1978): The crystal chemistry and petrogenesis of a magnesian rhodonite. *Am. Mineral*., **63**, 1137–1142.

Pinckney, L.R. & Burnham, C.W. (1988): High-temperature crystal structure of pyroxmangite. *Am. Mineral*., **73**, 809–817.

Prewitt, C.T. (1967): Refinement of the structure of pectolite, $Ca_2NaHSi_3O_9$. *Z. Kristallogr*., **125**, 298–316.

Schofield, P.F., Henderson, C.M.B., Cressey, G., van der Laan, G. (1995): 2*p* X-ray absorption spectroscopy in the earth sciences. *J. Synchrotron Radiat.*, **2**, 93–98.

Sheldrick, G.M. (1996): *SADABS*. University of Göttingen, Germany.

— (1997): *SHELXL-97*. A program for crystal structure refinement. University of Göttingen, Germany.

Tagai, T., Joswig, W., Fuess, H. (1990): Neutron diffraction study of babingtonite at 80 K. *Mineral. J.*, **15**, 8–18.

Takéuchi, Y. & Koto, K. (1977): A systematic of pyroxenoid structures. *Mineral. J.*, **8**, 272–285.

Takéuchi, Y., Kudoh, Y., Haga, N. (1973): The interpretation of partial Patterson functions and its application to structure analyses of sérandite $Mn_2NaHSi_3O_9$ and banalsite $BaNa_2Al_4Si_4O_{16}$. *Z. Kristallogr.*, **138**, 313–336.

Takéuchi, Y., Kudoh, Y., Yamanaka, T. (1976): Crystal chemistry of the serandite-pectolite series and related minerals. *Am. Mineral.*, **61**, 229–237.

Trojer, F.J. (1968): The crystal structure of parawollastonite. *Z. Kristallogr.*, **127**, 291–308.

Yamanaka, T., Sadanaga, R., Takéuchi, Y. (1977): Structural variation in the ferrobustamite solid solution. *Am. Mineral.*, **62**, 1216–1224.

Yamnova, N.A., Rastsvetaeva, R.K., Pushcharovskii, D.Yu., Mernaf, T., Mikheeva, M.G., Homyakov, A.P. (1992): Crystal structure of a new annular Na, K-silicate $Na_{16}K_2[Si_{18}O_{36}(OH)_{18}]\cdot 38H_2O$. *Kristallographiya*, **37**, 334–343 (in Russian).

Zanazzi, P.F., Nestola, F., Nazzareni, S., Comodi, P. (2008): Pryoxmangite: a high-pressure single-crystal study. *Am. Mineral.*, **93**, 1921–1928.

Received 5 October 2009
Modified version received 20 December 2009
Accepted 11 January 2010

Note added in proof

After the manuscript had been typeset we became aware that Schofield *et al.* (1995) explicitly stated that their Fig. 1 confirms that saneroite has an ideal formula with pentavalent vanadium. However, their saneroite X-ray absorption spectrum (their Fig. 1) shows a subordinate absorption maximum (at *ca.* 514 eV), which has been interpreted as V^{3+} characteristic absorption in other V-bearing minerals (Shofield *et al.,* 1995). Thus, our interpretation of V^{3+} in saneroite should be treated with reserve.